Conference paper

Selcuk Poyraz, Marissa Flogel, Zhen Liu and Xinyu Zhang*

Microwave energy assisted carbonization of nanostructured conducting polymers for their potential use in energy storage applications

Abstract: Three well-established one-step approaches, namely, conducting polymer (CP) nanofiber (NF) synthesis by NF seeding, CP nanoclip (NC) synthesis by oxidative template, and microwave (MW) energy-assisted carbonization were systematically combined to prepare carbonaceous nanostructures from CPs, with great potential as the active material for energy storage purposes. Polypyrrole (PPy), as one of the most well-known and commonly studied members of the CP family was prepared in both NF and NC forms, as the sacrificial carbonization precursor, for different property comparison purposes. Due to conducting polymers' high electron mobility and easily exciting nature under MW irradiation, both PPy NF and NC samples had vigorously interacted with MWs. The as-obtained carbonaceous samples from such interactions exhibited high thermal stabilities, competitive specific capacitance values and long-term stable electrochemical cyclic performances, which are crucial for the active materials used in energy storage applications. Thus, it is believed that, this well-established and well-studied process combination will dominate the large-scale manufacturing of the carbon-based, active energy storage materials from CPs.

Keywords: carbonization; conducting polymers; energy storage; microwave energy; nanostructures; POC-16.

Introduction

Along with the recently developed global awareness about the importance of sustainable energy, the growing potential of the next-generation hybrid or electric vehicles and the urgent demand for the daily use of widespread portable electronic devices, have significantly stimulated the researchers from both academia and industry to spend their efforts on the new energy storage technologies' development [1–4]. With respect to their desirable features such as low cost, pollution-free operation with high safety, long and stable cycling lifespan and high energy/power density, lithium ion batteries (LIBs) have been on the forefront of such key technologies as "the greenest and the most readily available secondary battery type" since their first release by Sony in 1991 [2, 4–7]. Like most of the other relevant technologies, this one also has its own common drawbacks such as low theoretical specific capacity (372 mAhg^{-1}) and low rate capability which tends to decay

---

*Corresponding author: Xinyu Zhang, Department of Chemical Engineering, Auburn University, Auburn, AL 36849, USA, Tel.: +1-334-844-5439, Fax: +1-334-844-4068, E-mail: xzz0004@auburn.edu
Selcuk Poyraz: Department of Chemical Engineering, Auburn University, Auburn, AL 36849, USA; and Department of Textile Engineering, Corlu Faculty of Engineering, Namik Kemal University, Corlu, Tekirdag 59860, Turkey
Marissa Flogel: Department of Chemical Engineering, Auburn University, Auburn, AL 36849, USA
Zhen Liu: Department of Chemical Engineering, Auburn University, Auburn, AL 36849, USA; Department of Physics and Engineering, Frostburg State University, Frostburg, MD 21532, USA; and Department of Materials Science and Engineering, University of Maryland, College Park, MD 20742-4111, USA

over time. In order to both improve the performance of these batteries for the large-scale energy demanding systems and to tackle the above mentioned challenges, the development of more efficient active materials is regarded as the most promising solution for this matter.

Carbonaceous materials with different morphologies, namely graphite, carbon nanotubes, porous nanofibers, hollow nano-spheres, etc. have been extensively utilized in commercial batteries for energy storage purposes [1–7]. The reason is basically related with the advantageous electrochemical properties of these materials which offer high coulombic efficiency, flat discharge voltage platform, and enhanced cycling performance that is free from Li-ion dendrite formation problem. Additionally, the porous nature of these nano-materials guarantees an enhanced battery performance via providing crucial kinetic advantages through a larger electrode/electrolyte interface for the electrochemical charge transfer reactions and a shortened diffusion pathway for the charge carriers [1–3, 7]. However, the common low electronic conductivity problem of such nano-materials restricts their overall performance in LIBs [2]. Here, the integration of a three-dimensional (3-D) conducting network morphology with a non-carbon element [nitrogen (N), boron (B), etc.] surface modification is offered as a rational solution to overcome this issue. Thus, carbon-based porous nano-materials with heteroatom-rich 3-D network morphology stand out among the other alternatives as the ideal option. Nanostructured CPs perfectly fit to this description owing to; (i) their chemical structure with high-level pyridinic N content, (ii) their densely packed morphology with ultra-high surface area, and (iii) their facile conversion into carbon at large-scale through different post-treatment methods like pyrolysis, hydrothermal carbonization or MW irradiation [1, 5–11].

In this study, PPy, as one of the most well-known and commonly studied members of the CP family, was selected and synthesized in both NF and NC forms via universal one-step methods. PPy in different nanostructures were used as the sacrificial carbonization precursor to prepare the active battery materials for different property comparison purposes [12–14]. Due to conducting polymers' high electron mobility and easily exciting nature under MW irradiation, both PPy NF and NC samples had vigorously interacted with MWs and the as-generated energy from such interactions was transformed into a large amount of heat leading to a drastic temperature increase, which was simultaneously used for the instant decomposition and carbonization of PPy nanostructures while preserving their morphological features [15–21]. In short, this combined process offers significant advantages such as; (i) being facile, easily scalable and affordable, (ii) being applicable at ambient conditions without the need of any extra equipment or chemical protection, and also (iii) being able to provide functional nano-carbons, without causing any distortion or physical alterations in the sacrificial nano-CP morphology. As a result, the as-obtained carbonaceous samples are meant to exhibit high thermal stabilities, competitive specific capacitance values and long-term stable electrochemical cyclic performances, which are crucial for the active materials used in energy storage applications. Thus, it is believed that this method possesses a promising potential for the large-scale preparation of the targeted materials with required properties for the above mentioned purposes.

Materials and methods

Materials

Hydrochloric acid (HCl, J.T. Baker), pyrrole (99 %, Alfa Aesar), acetone (J.T. Baker), cetyltrimethylammonium bromide [$(C_{16}H_{33})N(CH_3)_3Br$, CTAB, Amresco], ammonium peroxydisulfate [$(NH_4)_2S_2O_8$, APS, 98 %, Alfa Aesar], potassium hydroxide (KOH, Sigma Aldrich) and colloidal graphite paste (isopropanol base, Electron Microscopy Sciences) were all purchased and used as received. The V_2O_5 sol-gel NF was prepared based on a previously reported method [J. K. Bailey, G. A. Pozarnsky, M. L. Mecartney. *J. Mater. Res.* **7**, 2530 (1992)] by using ammonium metavanadate (NH_4VO_3, 99.5 %, Acros Organics) and Dowex Marathon (H) ion exchange resin (Sigma Aldrich) in DI water. Short-term MW energy-based carbonization of the nanostructured PPy samples was conducted on a standard kitchen countertop microwave oven (Panasonic Inverter NN-SN936B; 2.45 GHz

frequency, 120 V power source 60 Hz, 1250 W energy output, 1460 W energy input) with built-in time and power level controller.

One-step synthesis of PPy NF via seeding method

Based on a previously reported method, 1 mL of pyrrole monomer was gently added into 60 mL of 1 M aq. HCl under magnetic stirring. In order to obtain the homogenous dispersion of monomers, the medium was kept stirred for 10 min at ambient conditions. Next, 1 mL of V_2O_5 sol-gel NF seeds was gently introduced. This triggered the formation of well-dispersed nano-fibrous oligomers upon the preliminary oxidative interactions took place at the monomer/V_2O_5 NF seed interface. Within 30 s of the V_2O_5 seeds' addition, 1.15 g of APS was finally added into the mixture and instantly darkened its color as a clear indication of the oxidative polymerization reaction. After 4 h of polymerization reaction time under magnetic stirring at ambient conditions, the resulting dark precipitate of PPy NFs was suction filtered through a Buchner funnel while getting washed by copious amounts of HCl (3×100 mL) and acetone (3×100 mL), respectively. The damp PPy NF mesh was collected on a filter paper, placed in an oven at 80 °C and left in there overnight for drying purposes. Finally, the as-dried sample was gently crushed into smaller chunks and speed mixed in a capped plastic cup at 3500 rpm to gain its fine powder form.

One-step synthesis of PPy NC via oxidative template method

In a typical procedure, 0.01 M of CTAB (1.1 g) was dispersed in 100 mL 1 M aq. HCl in an ice bath. After magnetically stirred for 10 min, 0.03 M of APS (2.055 g) was added into this mixture and the stirring was continued for an additional 10 min until resulting into a white, cloudy precipitate of a CTAB/APS complex that would function as the oxidative template for pyrrole monomers' polymerization. The reaction medium was cooled down to 0–3 °C, and then 0.12 M of pyrrole monomer (2.4 mL) was added dropwise, without agitation. The polymerization reaction was allowed to proceed at this temperature for the next 24 h. The as-formed black precipitate of HCl doped PPy NCs was then suction filtered and washed by copious amounts of 1 M aq. HCl (3×100 mL) and acetone (3×100 mL), respectively. Next, the damp precipitate was collected on a filter paper, placed in an oven at 80 °C and left in there overnight for drying purposes. Finally, the as-dried sample was gently crushed into smaller chunks and speed mixed in a capped plastic cup at 3500 rpm to gain its fine powder form.

One-step preparation of nano-carbons from PPy NF and NC via MW energy-assisted process

In a typical procedure, 5 g of the as-synthesized PPy NF or NC sample was flatly spread on a watch glass or a petri dish for the following short-term MW energy-assisted carbonization process. As previously described in many similar studies, the sample was placed in the above mentioned MW oven chamber and then it was continuously exposed to 1250 W MW power for either 2 min, 5 min or 10 min, respectively. When MW power was turned on, continuous sparks were observed on the sample surface. During the process, the sample was turned to red hot and started glowing, as well. At the end, the sample was taken out of the MW chamber and left to cool down at ambient conditions. The cooled sample was then collected and stored for further characterization steps.

Characterization of the as-obtained nanostructures

The overall morphological features of the as-obtained nanostructures were analysed on a JEOL JSM-7000F scanning electron microscope (SEM) equipped with an energy-dispersive X-ray (EDX) detector. The thermal

stability change and solid residue wt.% of the nano-carbons were all determined via thermal gravimetric analysis (TGA), which was performed on a TA Q2000 instrument from room temperature up to 800 °C at 10 °C/min heating rate and under 40 mL/min N_2 flow. The changes took place in the major functional groups exist in the as-prepared nanostructures were detected by using a Thermo Nicolet 6700 Fourier Transform Infra-Red (FT-IR) spectroscope. The X-Ray diffractometry-based structural property confirmations and the UV-Visible light absorbance of the as-synthesized PPy nanostructures were obtained from Rigaku powder XRD and SHIMADZU UV-2450 spectrophotometer instruments, respectively.

Electrochemical characterization of the as-obtained nano-carbons

The materials should be prepared in homogeneous fine powder form prior to their use. Next, ~ 5 mg of the material was applied onto a mirror polished graphite electrode through the colloidal carbon paste. The as-prepared working electrode was then air-dried for 2 h before running the tests. The cyclic voltammetry (CV) tests were performed on a CHI-601D workstation equipped with a conventional three-electrode cell system. The as-prepared working electrode (WE) was used with a Pt wire as the counter (CE) and Ag/AgCl as the reference electrode (RE), respectively. 6 M aq. KOH solution was used as the electrolyte. CV was performed in sweeping voltage mode at 5 mV/s scan rate and within − 0.8 V to + 0.8 V potential window.

Results and discussion

In order to confirm the as-prepared samples' morphological features, they were first characterized by using electron microscopy technique. Figure 1 shows the as-obtained SEM results. The as-synthesized densely packed PPy NF network, decorated by nano-granular PPy clusters, is shown in Fig. 1a. These NFs were also proven to have inner nano-tubular cores (with an average ~ 6 nm diameter) due to their sacrificial V_2O_5 NF seeds' extraction from their cores by aq. HCl during the post purification step [22]. Figure 1b shows the as-synthesized PPy NCs with more and larger inter-molecular voids in their bundled structure. In Fig. 1c, the zoomed-in view of a few microns long PPy NFs can be seen with 60–75 nm in average diameter. The granular PPy nano-cluster decoration with 50–80 nm average diameters can be seen among these NFs, as well. Similarly, PPy NCs also have 50–75 nm average diameters with less nano-granular PPy decoration on their surface, as can be seen from Fig. 1d.

After 10 min continuous MW energy exposure of both PPy NF and NC samples, their morphological uniformity was remained almost the same, however, their elemental compositions were significantly changed as can be seen from Fig. 1e and f. The common morphological changes, such as larger intra-molecular pores and rougher surface area along the nanostructure axis, can be better observed in PPy NF samples compared to the NC ones. This phenomenon might be due to the difference in the initial carbon (C) and the dopant chloride ion (Cl^-) presence in PPy NF (C: ~ 57 %, Cl: ~ 15.5 %) and PPy NC (C: ~ 54.6 %, Cl: ~ 12.3 %) samples, from which their electrical conductivity is directly affected, and by which their reactivity in MW medium is determined [12, 14]. Moreover, the MW processed samples' elemental analysis results show that the C wt.% in their structures were increased up to 87 % for NCs and 95 % for NFs, respectively. It was also proven that such carbons were formed as adjacent graphitic layers with ~ 0.35 nm distance from each other [15, 18]. The as-obtained data from both SEM and EDX are quite consistent with the ones given in the relevant previous literature [16, 17, 23].

After the morphological and elemental analysis of the as-prepared samples, their thermal stability change and solid residue wt.% were also determined by using TGA and the results are shown in Fig. 2. Based on these results, it is understood that a significant improvement took place in MW processed samples' thermal stability features. As indicated with the arrows, a directly proportional relationship between the samples' thermal stability and their MW process time length can be clearly observed from both Fig. 2a and b. The plausible explanation of this situation should be correlated with the earlier mentioned "conversion of amorphous PPy
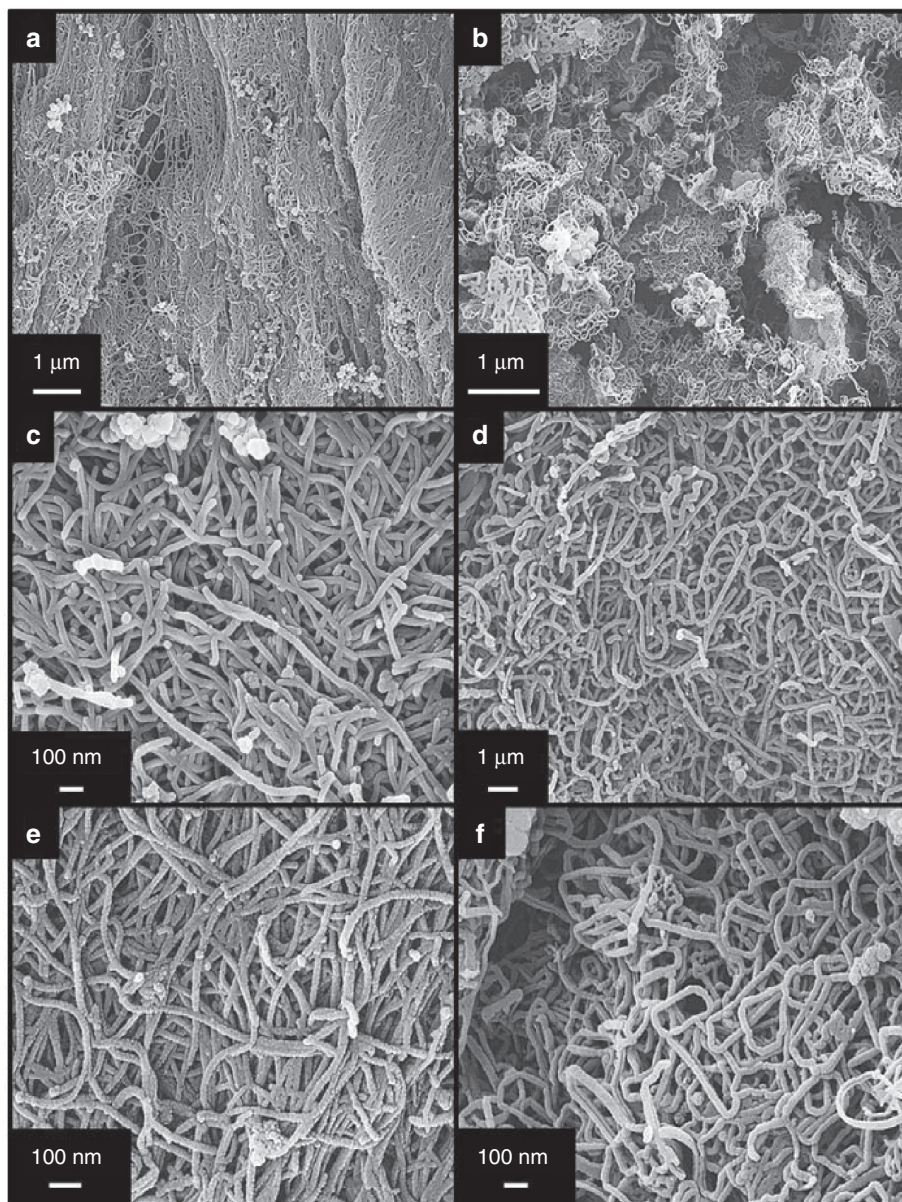
Fig. 1: SEM images of the PPy; (a) NFs, (b) NCs, (c) NFs'detailed view, (d) NCs'detailed view. SEM images of the carbonized; (e) NFs, (f) NCs after 10 min MW energy exposure.

into highly oriented graphitic carbon layers" whose rate is promoted by longer MW energy exposure time. This explanation is confirmed with the following results, as well. Here, PPy samples have gone through a major weight loss (~60–65%) up to 400 °C, whereas both of their 10 min MW processed versions' thermograms remained almost constant (only ~5–10% weight loss) at this temperature.

The change in PPy NF and NC's thermal stability and the major weight losses occurred in these samples are also shown in their derived TGA thermograms (Fig. 2c and d). According to these figures; a slight weight loss can be observed in both thermograms up to 100 °C, and this corresponds to the loss of moisture exists in the samples. The following two humps on the thermograms, centred around 250 °C and 350 °C, indicate the weight losses due to the removal of dopants or groups with small molecular weights attached to the primary PPy chains, and the beginning of primary PPy backbone chains' decomposition, respectively. The last hump on PPy NF and NC thermograms and the sharp peaks on their MW processed verisons' thermograms around 600 °C, indicate either the completion of PPy chains' or the as-formed carbonaceous samples' decomposition.
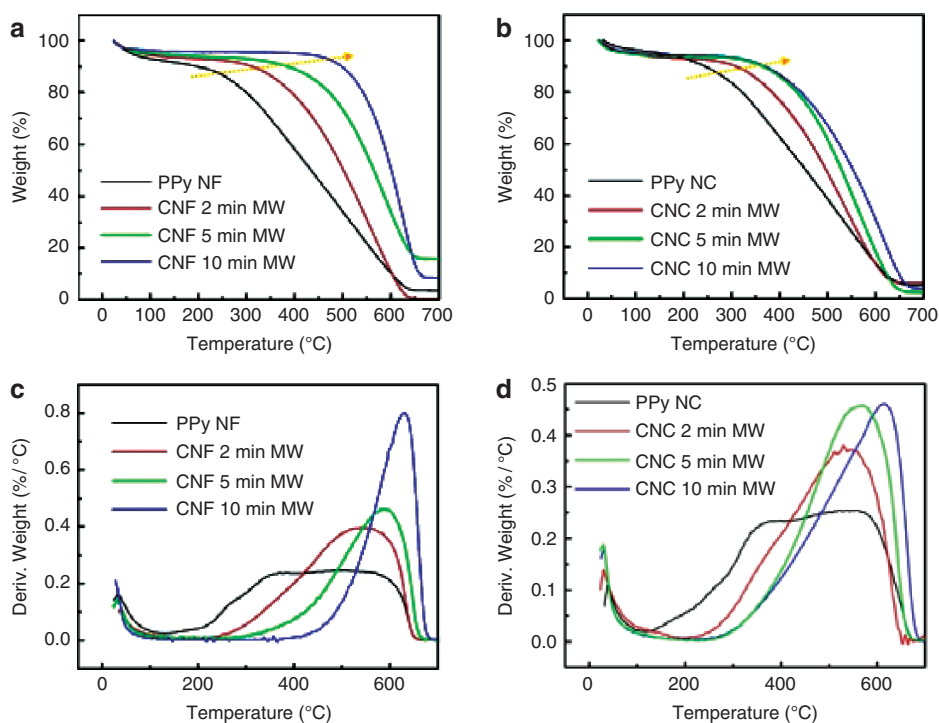
Fig. 2: Initial and derived TGA thermograms of the; (a, c) PPy NFs, (b, d) PPy NCs before and after MW energy exposure.

It should be noted that these sharp peaks' positions on the thermograms are shifted to higher temperatures along with their MW process time lengths.

The changes took place in the characteristic functional groups exist in the as-prepared samples, upon MW heating process, were detected by using FT-IR spectrometry and the results are shown in Fig. 3 and summarized in Table 1, as well. Quite compatible with the TGA results, the physicochemical changes occurred in PPy NF sample (Fig. 3a) can be more obviously observed than the ones in PPy NC (Fig. 3b). Here, such changes were revealed as broadening, overlapping, red shifting and even diminishing of the following characteristic functional groups' corresponding FT-IR peaks given in Table 1 [5, 7, 17–19].

The XRD-based structural property analysis and the UV-Vis light absorbance spectra of the as-synthesized PPy nanostructures are shown in Fig. 4a and b, respectively. The structural differences between these two nanostructures are clearly indicated by the XRD diffractograms in Fig. 4a. In good agreement with the other above mentioned material characterization results, the locally/partially crystalline nature of the PPy NC sample over the amorphous dominant structure of the PPy NFs can be easily differentiated by three sharp
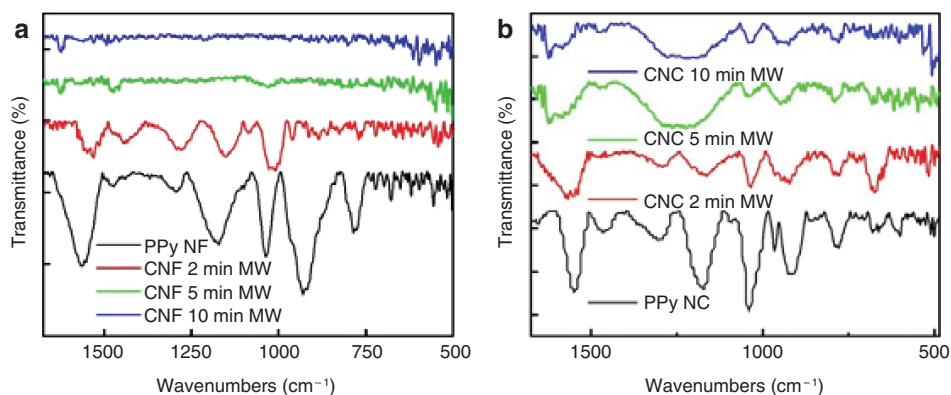
Fig. 3: FT-IR spectra of the; (a) PPy NFs, (b) PPy NCs before and after MW energy exposure.

**Table 1:** Summary of the common FT-IR spectra peaks detected in PPy NF and NC samples shown in Fig. 3.

Wavenumber (cm^{-1})	Definition
1550, 1545	Asymmetric C–C stretching vibration mode
	Secondary amine N–H peak
1490, 1470	Aromatic –C=C– stretching vibration mode
	Aromatic C–N stretching mode
1300, 1290	Symmetric vibration mode
	C–N$^+$–H stretching vibration mode in pyrrole ring
1180, 1170	Aromatic C–N stretching mode
	C–H in-plane vibration
1090	N–H in-plane vibration (doped state of PPy)
1040	C–H ring bending mode
960	C–H out-of-plane vibration
905	C–H out-of-plane vibration
780	C–H ring bending mode
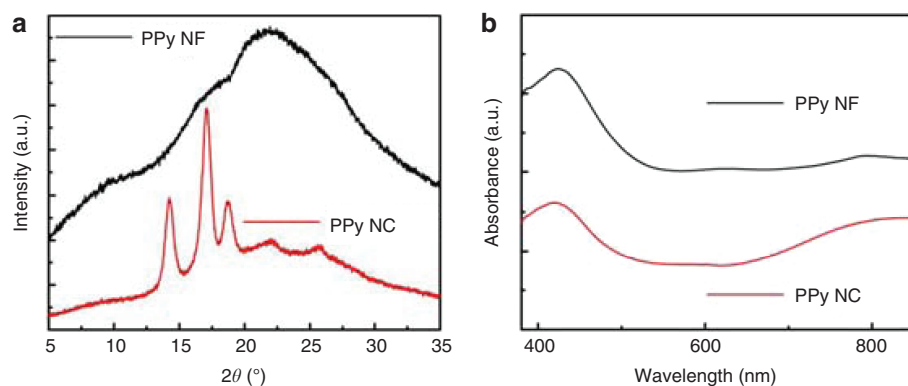
Fig. 4: (a) XRD diffractograms and (b) UV-Vis spectra of the sacrificial PPy NF and PPy NC samples obtained from one-step synthesis reactions.

peaks revealed on PPy NC diffractogram along with the overlapped broad shoulder-type ones on PPy NF's diffractogram. Here, compatible with the previous literature information, characteristic peaks centered at $2\theta = \sim 22°$ and $\sim 26°$ on both samples' diffractograms are ascribed to the scattering from amorphous PPy chains at the interplanar spacing [17, 24]. Providing another solid confirmation for the PPy nanostructures' synthesis, the UV-Vis spectra in Fig. 4b exhibit; (i) PPy's characteristic $\pi \rightarrow \pi^\star$ transition band at ~ 430 nm, (ii) a commencing tail from 650 nm, and (iii) a $\pi \rightarrow$ polaron transition band at ~ 850 nm, indicating the oxidized PPy presence in conducting form in both samples [17, 25].

The success of both PPy NF's and NC's one-step synthesis reactions and their nano-carbon counterparts' preparation through short-term MW energy-assisted heating process has been adequately proven by the material characterization results given so far. Lastly, the as-prepared materials' application performance potentials were also evaluated via the following electrochemical test results given in Fig. 5. The double layer region (− 0.4 V to 0.4 V) and the oxide formation region (0.4 V–0.8 V) can be clearly observed as the common major regions from both PPy NF and NC samples' voltammograms in Fig. 5a [17–19]. Along the anodic scans of both samples' voltammograms there were two peaks formed within these regions, at ~ − 0.2 V (for PPy NF), ~ 0 V (for PPy NC) and ~ 0.8 V (for both), respectively. The electrochemical procedure that took place on the PPy NF and NC electrode surfaces was described by those peaks (with apparently broader shapes in PPy NF's voltammogram) as shown in Fig. 5a. Here, the first anodic peaks (− 0.2 V and 0 V) represent the electrolyte chemisorption through the nano-material on the electrode surface. After this peak, the current density value was remained longer in PPy NF-based electrode than the one in PPy NC-based. This is a clear indication of an unsaturated adsorption, which was synergistically supported by PPy NFs' superior morphological features
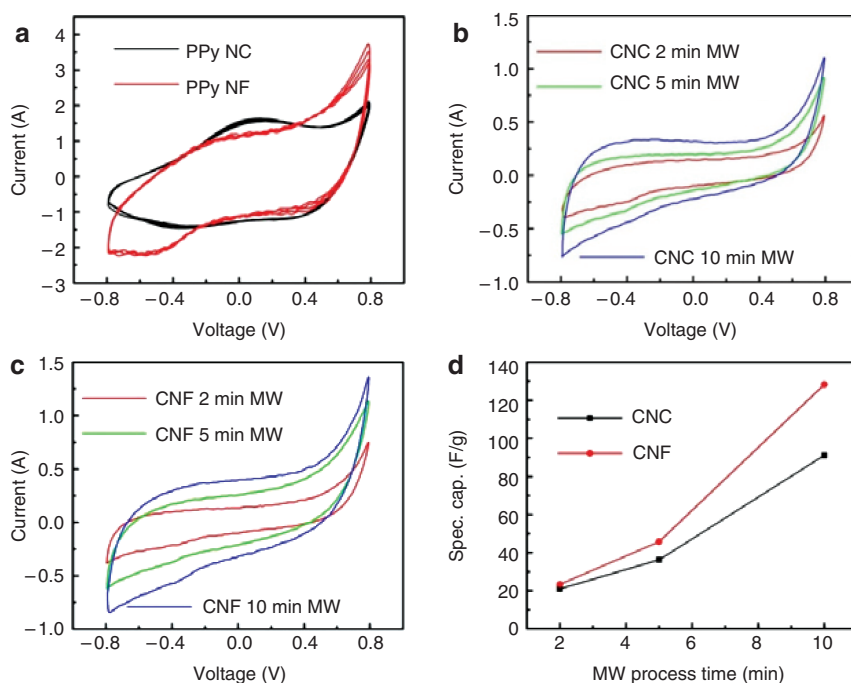
Fig. 5: CV voltammograms of the; (a) PPy NFs and NCs (1000 cycles), (b) CNCs, (c) CNFs after MW energy exposure, and (d) MW processed samples' specific capacitance value summary.

with larger porous surface area and inner nano-tubular core. The following anodic peak (0.8 V) was formed due to the reactive sites' oxidation on the electrode surface. Beyond this potential value, both electrodes' oxidation activities were stopped and this caused a sharp decrease in their current values. Two distinctive peaks, located at ~ 0.4 V (for both) and ~ − 0.4 V (for PPy NC), ~ − 0.5 V (for PPy NF), respectively, can be also observed on the same voltammograms' cathodic scans. Here, the first peak (0.4 V) indicates the previously formed oxidized reactive surface sites' reduction, while the final peaks (− 0.4 V, − 0.5 V) represent the electrolyte desorption from the nano-materials attached to the electrode surface [17–19]. In summary, both the consistency in anodic/cathodic peak locations at the corresponding electrode materials' voltammograms during 1000 consecutive cycles, and the highly stable responses generated by these electrodes clearly represents the long-term stability of their electrochemical working mechanism, which is based on the surface adsorption/desorption of the alkaline electrolyte through the active PPy nano-materials on their surfaces.

After the MW energy-based heating process, the as-obtained carbonized nanostructures' CV voltammograms are shown in Fig. 5b and c, respectively. In good agreement with this situation, these nano-materials' electrochemical characteristics were significantly changed. As it can be seen in both figures, the above explained PPy CVs with Faradaic redox peaks were replaced by "quasi-rectangular" voltammograms, which indicate their new capacitive features [15, 26]. This change was also backed up by the hydrogen adsorption region's (− 0.8 V to − 0.4 V) more dominant appearance in the new voltammograms [17]. Here, the as-formed graphitic carbon layers in both MW processed samples have successfully served as the current collectors and provided pathways for the free electrons' transportation [26]. Additionally, the clear consistency between the voltammogram area and the MW process time length of the sample can be readily observed in both materials' results. Apparently, CNF samples have reached higher current values and generated larger voltammograms compared to the CNC ones. The reason should be simply related with the "synergistic effect" caused by the co-existence of graphitic carbon layers and the inner nano-tubular core in CNF samples, through which, the extra electrolyte storage routes and graphite's intercalation-based electrochemical working mechanism are simultaneously provided [1, 15, 22]. Such morphological structure obtained through the MW heating process offers the noteworthy advantages of larger active surface area, lowered resistance, improved electrolyte utilization efficiency and enhanced capacitive property to this sample, as well [3, 19].

Since the electrodes are composed of active graphitic carbonaceous material, their working mechanism represents ordinary electric double-layer (EDL) feature that is based on the formation/decomposition of solid electrolyte interface (SEI) and the insertion/extraction of the electrolyte through their nano-scale porous structure [26]. Thus, the initial anodic peak around – 0.6 V and the following flat plateau between – 0.4 V and 0.4 V indicate these steps, respectively. The final sharp peaks along the anodic scan, around 0.8 V, point to the oxidation process's completion on the electrode surface. During the subsequent cathodic scan, the broad peaks at 0.6 V are related to the electrolyte reduction. Next, the small deflection around – 0.4 V and the final sharp peaks at – 0.8 V correspond to the electrolyte's extraction from the defective carbonaceous materials' structure and the previously formed SEI layers' decomposition, respectively.

The overall similarity between these electrodes' unchanged CV responses with long-term cycling stability clearly proves that their active materials do have the identical graphitic carbon composition, but they do not have a common structure due to their morphological differences [3]. The electrodes' specific capacitance values were also calculated from the electrochemical test results and their summary is shown in Fig. 5d. This result provides another strong support for the advantageous contribution of the inner nano-tubular core (~ 130 F/g) over the solid NC version (~ 90 F/g) on the same materials' capacitive performance. In short, it could be understood that the as-prepared active carbonaceous nano-materials exhibit a quite competitive electrochemical performance and have a promising application potential as the active energy storage materials.

Conclusion

Conducting PPy NF and NC samples with high electron mobility and easily exciting nature under MW irradiation were obtained from well-established and well-studied universal one-step synthesis methods and then served as templates to prepare active carbonaceous nano-materials that can be effectively used in energy storage applications via facile, simple and easily scalable short-term MW heating process. Both nano-materials retained their relevant morphological features, which had positively contributed to their electrochemical application performance potentials. Various advanced material characterization test results and the electrochemistry-related calculations have provided strong supports for the; (i) as-applied nanostructured material synthesis/preparation methods' success and their advantages, (ii) MW processed samples' improved thermal stabilities, (iii) graphitic carbon-based structure and inner nano-tubular core's synergistic effect on CNF sample's properties, and (iv) CNF sample's superior energy storage application performance potential over the CNC one due to its morphological advantages. The as-prepared nanostructured samples' unchanged electrochemical characteristics (remained constant after 1000 cycles) and their improved specific capacitance values (from ~ 25 F/g up to ~ 130 F/g) along with their MW process time length (from 2 min to 10 min) should be also mentioned as the other clear evidences for the success of this combined material preparation process. Thus, it is believed that this promising process will soon be commonly used to prepare active carbonaceous materials from nanostructured CPs in large scale, for the advanced energy storage applications.

References

[1] L. Qie, W. M. Chen, Z. H. Wang, Q. G. Shao, X. Li, L. X. Yuan, X. L. Hu, W. X. Zhang, Y. H. Huang. *Adv. Mater.* **24**, 2047 (2012).
[2] S. Xin, Y. G. Guo, L. J. Wan. *Acc. Chem. Res.* **45**, 1759 (2012).
[3] M. H. Wu, J. Chen, C. Wang, F. Q. Wang, B. L. Yi. *Electrochim. Acta* **105**, 462 (2013).
[4] C. de las Casas, W. Z. Li. *J. Power Sourc.* **208**, 74 (2012).
[5] Z. H. Wang, X. Q. Xiong, L. Qie, Y. H. Huang. *Electrochim. Acta* **106**, 320 (2013).

[6] J. Yang, X. Y. Zhou, J. Li, Y. L. Zou, J. J. Tang. *Mater. Chem. Phys.* **135**, 445 (2012).

[7] X. Y. Zhou, J. J. Tang, J. Yang, J. Xie, B. Huang. *J. Mater. Chem. A* **1**, 5037 (2013).

[8] J. H. Zhu, S. Pallavkar, M. J. Chen, N. Yerra, Z. P. Luo, H. A. Colorado, H. F. Lin, N. Haldolaarachchige, A. Khasanov, T. C. Ho, D. P. Young, S. Y. Wei, Z. H. Guo. *Chem. Commun.* **49**, 258 (2013).

[9] M. M. Titirici, M. Antonietti. *Chem. Soc. Rev.* **39**, 103 (2010).

[10] U. Riaz, S. M. Ashraf. *RSC Adv.* **4**, 47153 (2014).

[11] U. Riaz, S. M. Ashraf. *Appl. Clay Sci.* **52**, 179 (2011).

[12] X. Y. Zhang, S. K. Manohar. *J. Am. Chem. Soc.* **126**, 12714 (2004).

[13] Z. Liu, Y. Liu, S. Poyraz, X. Y. Zhang. *Chem. Commun.* **47**, 4421 (2011).

[14] Z. Liu, X. Y. Zhang, S. Poyraz, S. P. Surwade, S. K. Manohar. *J. Am. Chem. Soc.* **132**, 13158 (2010).

[15] X. Y. Zhang, S. K. Manohar. *Chem. Commun.* **23**, 2477 (2006).

[16] X. Y. Zhang, Z. Liu. *Nanoscale* **4**, 707 (2012).

[17] Y. Liu, N. Lu, S. Poyraz, X. L. Wang, Y. J. Yu, J. Scott, J. Smith, M. J. Kim, X. Y. Zhang. *Nanoscale* **5**, 3872 (2013).

[18] Z. Liu, Y. Liu, L. Zhang, S. Poyraz, N. Lu, M. Kim, J. Smith, X. L. Wang, Y. J. Yu, X. Y. Zhang. *Nanotechnology* **23**, 335603 (2012).

[19] Z. Liu, S. Poyraz, Y. Liu, X. Y. Zhang. *Nanoscale* **4**, 106 (2012).

[20] S. Poyraz, L. Zhang, A. Schroder, X. Y. Zhang. *ACS Appl. Mater. Interfaces* **7**, 22469 (2015).

[21] U. Riaz, S. M. Ashraf, M. Aqib. *Arab. J. Chem.* **7**, 79 (2014).

[22] X. Y. Zhang, S. K. Manohar. *J. Am. Chem. Soc.* **127**, 14156 (2005).

[23] F. D. Han, Y. J. Bai, R. Liu, B. Yao, Y. X. Qi, N. Lun, J. X. Zhang. *Adv. Energy Mater.* **1**, 798 (2011).

[24] M. A. Chougule, S. G. Pawar, P. R. Godse, R. N. Mulik, S. Sen, V. B. Patil. *Soft Nanosci. Lett.* **1**, 6 (2011).

[25] H. Shigi, M. Kishimoto, H. Yakabe, B. Deore, T. Nagaoka. *Anal. Sci.* **18**, 41 (2002).

[26] P. Y. Li, J. C. Deng, Y. Li, W. Liang, K. Wang, L. T. Kang, S. Z. Zeng, S. H. Yin, Z. G. Zhao, X. G. Liu, Y. Z. Yang, F. Gao. *J. Alloys Compd.* **590**, 318 (2014).